Physics Letters A 384 (2020) 126658

Contents lists available at ScienceDirect

Physics Letters A

www.elsevier.com/locate/pla

Theoretical investigation of $V_{2x}Fe_{2(1-x)}Zr$ and $Sc_xY_{1-x}Fe_2$ (0<x<1) quasi-binary alloy: Stable structures, mechanical and electronical properties

Yong-Lin Jiang [a], Yu-Zhu Chen [c], Hui Wang [c], Xiao-Bao Yang [a,b,*]

[a] Department of Physics, South China University of Technology, Guangzhou, 510640, People's Republic of China
[b] Key Laboratory of Advanced Energy Storage Materials of Guangdong Province, South China University of Technology, Guangzhou, 510640, People's Republic of China
[c] School of Materials Science and Engineering and Guangdong Provincial Key Laboratory of Advanced Energy Storage Materials, South China University of Technology, Guangzhou 510641, People's Republic of China

ARTICLE INFO

Article history:
Received 18 January 2020
Received in revised form 28 May 2020
Accepted 6 June 2020
Available online 17 June 2020
Communicated by L. Ghivelder

Keywords:
Quasi-binary alloy
Structural stability
Phase transition
Mechanical properties
First-principles calculations

ABSTRACT

Combining experimental XRD phase analysis and melting-annealing temperature with the high-through first-principles calculation, the structural stability, mechanical strength and electronic properties of V-Fe-Zr and Sc-Fe-Y quasi-binary alloys have been systematically investigated. The calculation of formation enthalpy and the free energy show that $V_xFe_{2(1-x)}Zr$ alloy has a completely ordered solid solution at low temperature, while $Sc_xY_{1-x}Fe_2$ alloy needs to be annealed at a high temperature up to 700 °C to reach disordered fusion state. The bond energy model can accurately predict the total energy and bulk modulus of the target alloy structure at each substitution concentration, whose numerical differences per atom between the calculated results and predicted ones by bond energy model (BEM) are less than 1 meV and 0.2 GPa, respectively. The elastic modulus obtained by fitting within Birch-Murnaghan equation and calculating from elastic constants has good consistency.

1. Introduction

Quasi-binary alloy with the compositional control is often used in the design for high-entropy alloy [1], which has become the main manipulation to develop high-performance metal materials nowadays. The calculated phase diagram, combining the statistical principle and the first-principles method, plays an important role in providing theoretical guidance and reducing operating costs for the experimental preparation of alloys. It is an evolving approach applicable widely to screen out the stable ground state structure under a specific stoichiometry and a lattice type [2], where the phonon spectrum [3], binding energy [4], and mechanical parameters [5] have also been studied to evaluate the stabilities. The casting of alloys is microscopically formed as a solid solution or intermetallic compound, in which the heterogeneous atoms replace the substrate lattice atoms or occupy the interstitial positions respectively. The solubility mainly depends on crystal structure [6], atomic size, electronegativity, electron concentration [7] and so on.

In alloy system, the Laves phase has a close-packed nature whose typical complex cubic unit structure (C15) consists of 24 atoms with only tetrahedral closed-packed interstitial [8]. In this alloy, there are three kinds of tetrahedron cited as B_4 (composed of four smaller B-atoms), A_1B_3 (composed of one A-atom and three B-atoms), A_2B_2 (composed of two A-atom and two B-atoms), with the number [9,10] of 8, 32, and 96 respectively. With a great number of interstitials for high uptakes of hydrogen atoms and high mechanical strength, the Laves alloy family has been proved to be a potential application of hydrogen storage [11], while it should be paid attention to the YFe_2 with C15 lattice due to an inhibition of disproportionation reaction [12] and hydrogen amorphization [13] at high hydrogen storage.

To achieve high elastic modulus and smaller weight, the replacement of Y atoms by the Sc atoms, or the replacement of Fe atom by V atom, is supposed to update relative alloy performance requirements. S. Banerjee et al. [14] found the structure migration occurred in the $V_xFe_{2-x}Zr$ alloy system obtained by an arc melting and water cooled treatment with different V components at x=0.2, 0.4, 0.6, 0.8 via an X-ray diffraction profile under same conditions. Cao et al. [15] carried out similar works in system $V_xFe_{2-x}Zr_{1.04}$ about x=0.1, 0.2, 0.3, 0.5. Budzyński et al. [16] gave a XRD pattern representative of $Y_{1-x}Sc_xFe_2$ (x=0.0, 0.2, 0.5,

* Corresponding author at: Department of Physics, South China University of Technology, Guangzhou, 510640, People's Republic of China.
E-mail address: scxbyang@scut.edu.cn (X.-B. Yang).

https://doi.org/10.1016/j.physleta.2020.126658
0375-9601/

0.7, 0.8, 1.0) with larger substitution ranges. In their characterization, the phase transformation was proposed from cubic C15 to hexagonal C14 arisen with the increasing of vanadium content. Despite of the $ZrFe_2$ and ZrV_2 pure binary phase alloys studied by first-principles calculations in literatures [17–19], it is still a challenge to consider the $V_{2x}Fe_{2(1-x)}Zr$ with monotonic intermediate component due to numerous isomers. Therefore, it is important to systematically investigate the structural stability of quasi-binary alloys of the $Sc_{2x}Y_{1-x}Fe_2$ and $V_{2x}Fe_{2(1-x)}Zr$ with higher entropy, in order to obtain a ternary alloy with specific components and better performance.

In order to investigate the average energy held on neighbor ion pairs among different components and the regularity of ion distribution in the alloy solid solution, the cluster expansion method based on the bond energy model was applied in this study. By a comparison of the effective cluster interaction coefficients between the nearest neighbor items, and of a histogram statistic of energy difference between the results from DFT calculation with that from cluster expansion prediction, it is found that the cluster expansion model established can be reasonable for the prediction of total energy of target alloy, which is meaningful to the energy evaluation of supercell with a larger number of nonequivalent structures, for the sake of prevention of computational cost and the improvement of computational efficiency. Stable structures with various stoichiometries are determined by the formation energy with the convex analysis. We have also discussed the elastic property, bonding strength and the free energy about high-temperature disorder phase boundary. Our calculations will be of importance to provide a theoretical support for the practical preparation and applications of target alloys.

2. Calculation details

2.1. First-principles calculation

The first-principles calculations have been performed using the Vienna *Ab-initio* Simulation Package (VASP) [20]. Projector augmented wave potentials were utilized to parameterize the generalized-gradient approximation (GGA) within Perdew, Burke, and Ernzerhof (PBE) scheme [21]. The $7 \times 7 \times 7$ k-mesh in the irreducible Brillouin zone and the cut-off energy as 450 eV were adopted after a convergence test respectively. The spin polarized calculation was considered for all alloy structures, where the relaxation was fully conducted until the total forces on each atom were smaller than 0.02 eV/Å. For the implementation of measurement of XRD data carried out by our cooperative experimental research group, X-ray diffraction analysis (XRD equipment, Rigaku MiniFlex 600) was completed with Cu-Kα radiation ($\lambda = 0.15406$ nm) at 45 kV and 40 mA (PANalytical Empyream).

2.2. Structural recognition

For the $M_xA_{1-x}B$ alloy system (M is considered as a heterogeneous atom substituted), the mutual substitution components generally are in a same lattice structure to ensure a higher solid solubility during practical fusion process. In the alloy structure (ZrV_2 and YFe_2) as the conventional AB_2 Laves substrate, the A-side (Y and Zr) and B-side (V and Fe) metal element has a same close-packed hexagonal structure (hcp) and a same body-centered cubic (bcc) structure respectively. The number of possible structures composed of $Sc_xY_{1-x}Fe_2$ and $V_{2x}Fe_{2(1-x)}Zr$ is respectively 2^8 and 2^{12} because the alternative ions within the two cell systems is 8 and 12 that obtained from an extension operation from their primitive cell in a same configuration. Afterwards, removing the equivalent structures by the structural recognition, 14 and 290 cell structures were obtained in the selected lattice, whose total energies were calculated by the first-principles method.

2.3. Formation enthalpy and free energy

The formation enthalpy E_f for a given structure $M_xA_{1-x}B$ is defined as follows [22,23]:

$$E_f = E_t - X_{MA} \times E_{MA} - (1 - X_{MA}) \times E_{MB} \quad (1)$$

Here E_t is the total energy of $M_xA_{1-x}B$, X_{MA} is ratio of variable atoms to their sum, E_{MA} and E_{MB} is the energy of unsubstituted end-point cell structure for both two sides.

The free energy based on the partition function [24] is given as:

$$F = -kT \ln \sum_l \omega_l e^{-\beta \varepsilon_l} \quad (2)$$

Where $\beta = 1/kT$, k and T is the Boltzmann constant and temperature, ω_l and ε_l is degeneracy and energy level.

3. Results and discussion

3.1. Structural stabilities

The negative formation enthalpy indicates a high structural stability for the given alloy system. For the structures with positive formation enthalpy, the contribution of configuration entropy to the free energy of alloy system is necessary to be considered at higher temperature. Fig. 1(a), (c) shows the calculated formation enthalpies of $V_{2x}Fe_{2(1-x)}Zr$ and $Y_{1-x}Sc_xFe_2$ with typical structures, the former of which possesses the negative formation enthalpies for certain stoichiometry at T=0 K. However, the formation enthalpies for the $Y_{1-x}Sc_xFe_2$ are found to be all positive, which will be separated into two phases at low temperature. Fig. 1(b), (d) shows the variation of free energies as a function of temperature. For $V_{2x}Fe_{2(1-x)}Zr$, there are three stable structures according to the convex-hull analysis, and the number of stable structures with various concentrations grows as the temperature increases. With the temperature lower than 300 °C, the formation enthalpies of most $Y_{1-x}Sc_xFe_2$ are found to be positive while E_f will become negative when the temperature is 500 °C, which is in agreement with the experimental results that stable solid solutions of $Y_{1-x}Sc_xFe_2$, have been observed with the annealing over 700 °C.

For the $Sc_xY_{1-x}Fe_2$ alloy, in order to obtain the finally stable single-phase C15 structure at low temperature, it is necessary to undergo an annealing process after high-temperature melting to remove the heterogeneity. A stable C15 cubic structure can be obtained at all Sc contents. According to Bragg Law ($2d \sin\theta = n\lambda$) and Vegard's Law ($a = a_Y + (a_{Sc} - a_Y) \times X_{Sc}$) in the solid solution alloy, smaller atom radius of Sc than that of Y atom causes a larger Bragg angle, thus the diffraction peak shifts to the right (Fig. 2).

3.2. Bond energy model and electronic properties

The expression of bond energy model (BEM) for the A_xB_{1-x} alloy in terms of pair and many-body interactions is given as below [25],

$$E_{BEM} = \sum n_{ii} J_{ii} + \sum n_{jj} J_{jj} + \sum n_{kk} J_{kk} + \sum n_{ij} J_{ij} \ldots \quad (3)$$

Where n_{ii}, n_{jj} and n_{ik}, ... are sequentially the total number of AA, BB, AB bonds in the alloy crystal, J_{ii}, J_{jj} and J_{ik}, ... are the energy coefficients of these bonds, respectively. For $V_{2x}Fe_{2(1-x)}Zr$, we have used 289 structures to fit the parameters in BEM as shown in Fig. 3(a) and (b). There is a linear dependence of the calculated total energies from DFT on those from BEM and the

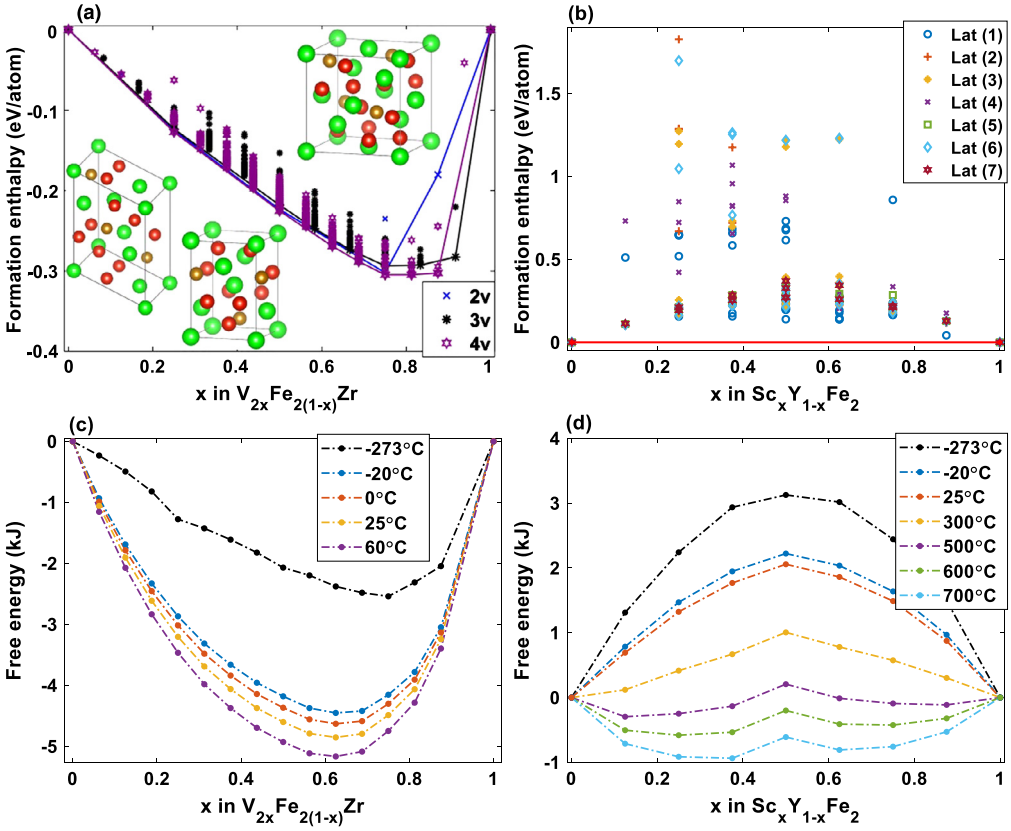

Fig. 1. (a) Formation enthalpies of $V_{2x}Fe_{2(1-x)}Zr$ alloy systems obtained from one structure of 2, 3, 4 times of primitive cell structures and three convex-point structures with lowest formation energy; (b) Formation enthalpies of $Y_{1-x}Sc_xFe_2$ alloy systems obtained from 7 types of lattice all (shown in Fig. 2(b)) 4 times of primitive cell, the green, golden, and red pellet is respectively representing Zr, Fe, and V atoms; (c) Free energy variable with the substitution concentration under different temperatures for $V_{2x}Fe_{2(1-x)}Zr$ systems with a wholly negative value range; (d) Free energy for $Y_{1-x}Sc_xFe_2$ systems while possessing positive results as the temperature lower than 500 °C. (For interpretation of the colors in the figure(s), the reader is referred to the web version of this article.)

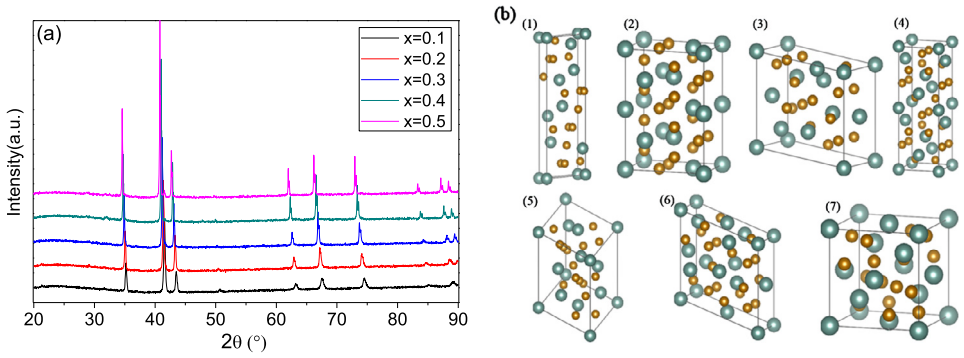

Fig. 2. (a) XRD patterns of $Y_{1-x}Sc_xFe_2$ products (x = 0.1, 0.2, 0.3, 0.4, 0.5) after high-temperature annealing; (b) The crystal structures with a same volume expanded from one primitive cell, larger cyan spheres stand for Y atoms whereas the brassy ones for Fe atoms.

test error is 0.0081 meV per atom. For $Y_{1-x}Sc_xFe_2$, 14 structures are used and the test error is found to be 0.00103 meV per atom. Thus, the total energies of $V_{2x}Fe_{2(1-x)}Zr$ and $Y_{1-x}Sc_xFe_2$ can be well described by the bond energy model, which can be further used to search the stable alloy.

The bond energy parameters classified in the first nearest neighbor can describe the bonding strength among the atoms. The binding energy of V and Fe to the Zr atom is dominant to the total energies (Fig. 4(a)). For V and Fe atoms, the binding energy between V and Fe atoms satisfies the expression in $2 \times E_{V-Fe} < E_{V-V} + E_{Fe-Fe}$, indicating that the substitution of V atoms for Fe atoms can reduce the total energy of the alloy structure and enhance the stability of alloy system.

To demonstrate the atomic bonding, we have used the electron localization function (ELF) [26] to represent charge density distribution [27] as shown in Fig. 4(b), where (1) (2) (3) is the selected lattice plane passing through three types of atom in the crystal structure, but (4) (5) (6) is the front view of the selected lattice plane in which contour lines were plotted to separate associated color that represents the electron localization extent. The maximum and minimum value of ELF function is shown in red and blue respectively, while the green domain denotes equal distribution of the electron cloud. Hence the electrons of Zr atom are found to be localized, while those of the V and Fe atoms are delocalized. Compared to Fe atoms, the electrons of V atoms are more delocalized (with larger area of blue region shown in Fig. 4(b)), indicating the

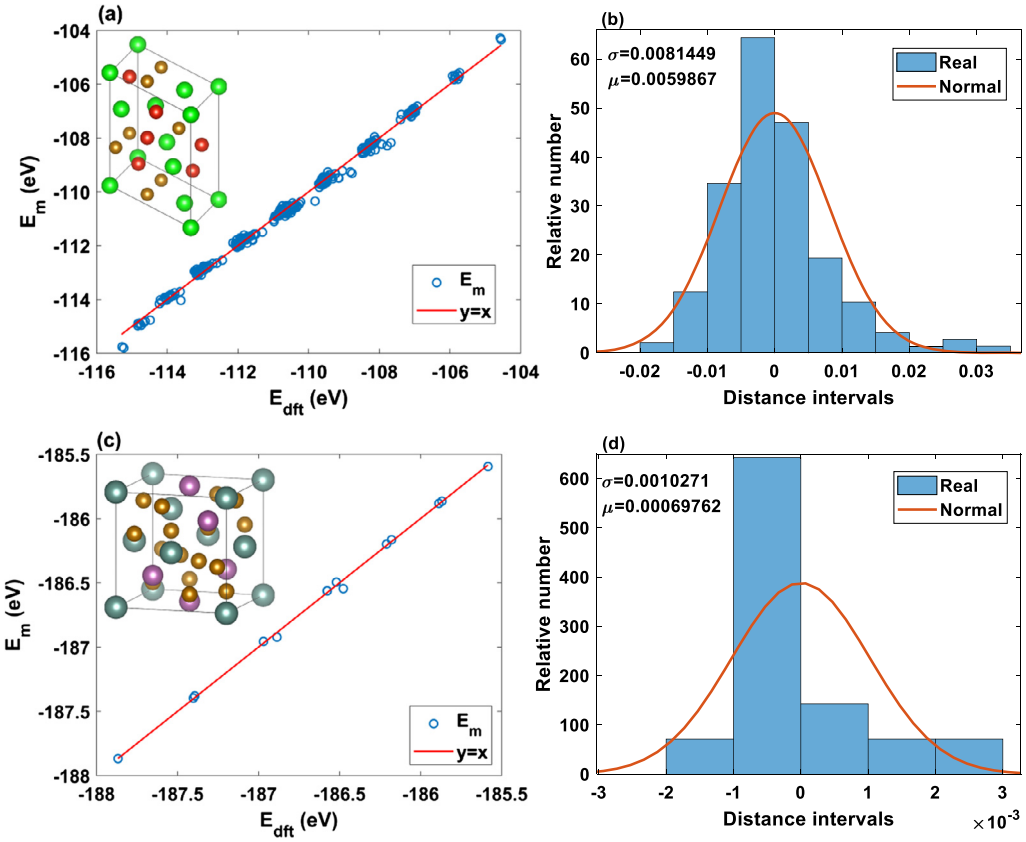

Fig. 3. Total energies of $V_{2x}Fe_{2(1-x)}Zr$ (a) and $Y_{1-x}Sc_xFe_2$ (c) (Purple pellet on behalf of the S_c atom) systems obtained by DFT calculation (red line) and by BEM method (blue circle); (b) Histogram distribution of numeric differences between the energy calculated from DFT and that from BEM for $V_{2x}Fe_{2(1-x)}Zr$ system with fitted normal curve, standard deviation (σ) and average (μ) are shown in top-left corner; (d) Analogous distribution characteristic of total energy difference for $Y_{1-x}Sc_xFe_2$ systems.

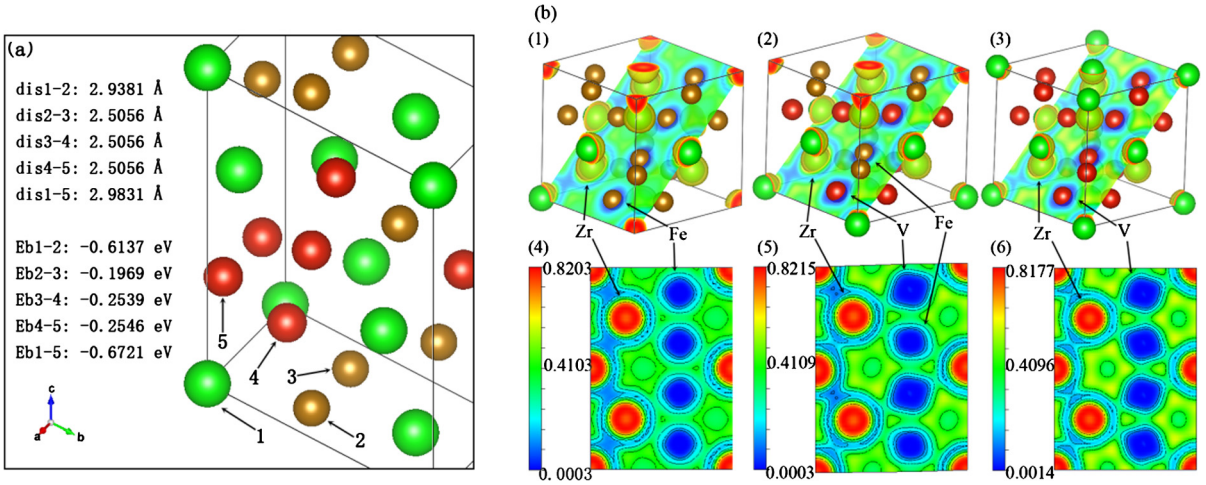

Fig. 4. (a) Distance and energy among V, Fe, and Zr three atoms within first neighbor in the supercell of 3 times primitive cell (dis1-2 represents the interatomic distance between the Zr and Fe atoms, and E_{bond}1-2 the interatomic energy between the Zr and Fe atoms, subsequently); (b) Electron localization function maps along the {1 0 −1} planes. Black arrow labels 3 kinds of atoms in the parallel lattice planes that is existed in the structure and is extracted as the front view.

stronger bonding of V-Zr atoms. Fig. 5 shows the density of states (DOS) for the stable structures based on the convex-hull analysis, which are metallic because of the large states near the Fermi surface. With the introduction of V atoms, the *d*–orbital hybridization among V, Fe and Zr irons obviously leads to an enhancement in the strength to metal bond in the alloy systems. Moreover, the DOS peaks of V and Zr atoms are more overlapped than those of Fe atoms. Thus, the bonds of V and Zr atoms are stronger than those of Fe and Zr, which is consistent with the energy parameters in BEM shown in Fig. 4(a).

3.3. Elastic properties

The Birch-Murnaghan (BM) equation [28,29] and elastic constants [30–34] are commonly used to evaluate elastic strength of target alloy structures by virtue of Voigt-Hill approximation and a fitting on crystal equilibrium condition. The calculated elastic properties of $V_{2x}Fe_{2(1-x)}Zr$ alloy system with BM fitting are shown in Fig. 6, where 9 stable structures at a specific V concentration were relaxed fully by an external pressure. The total energies and pressures as a function of volume can be well fit with BM equations,

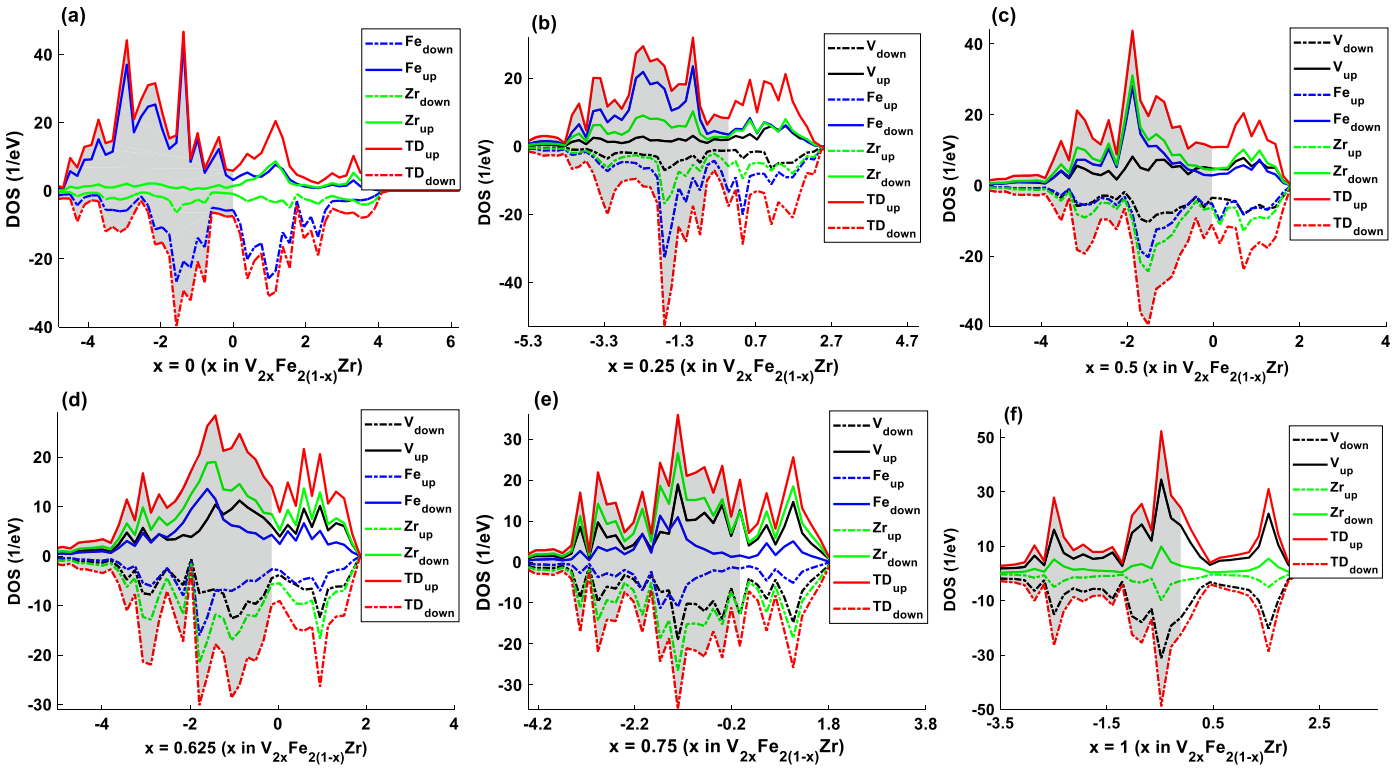

Fig. 5. Total and partial DOS of $V_{2x}Fe_{2(1-x)}Zr$ selective cell structures.

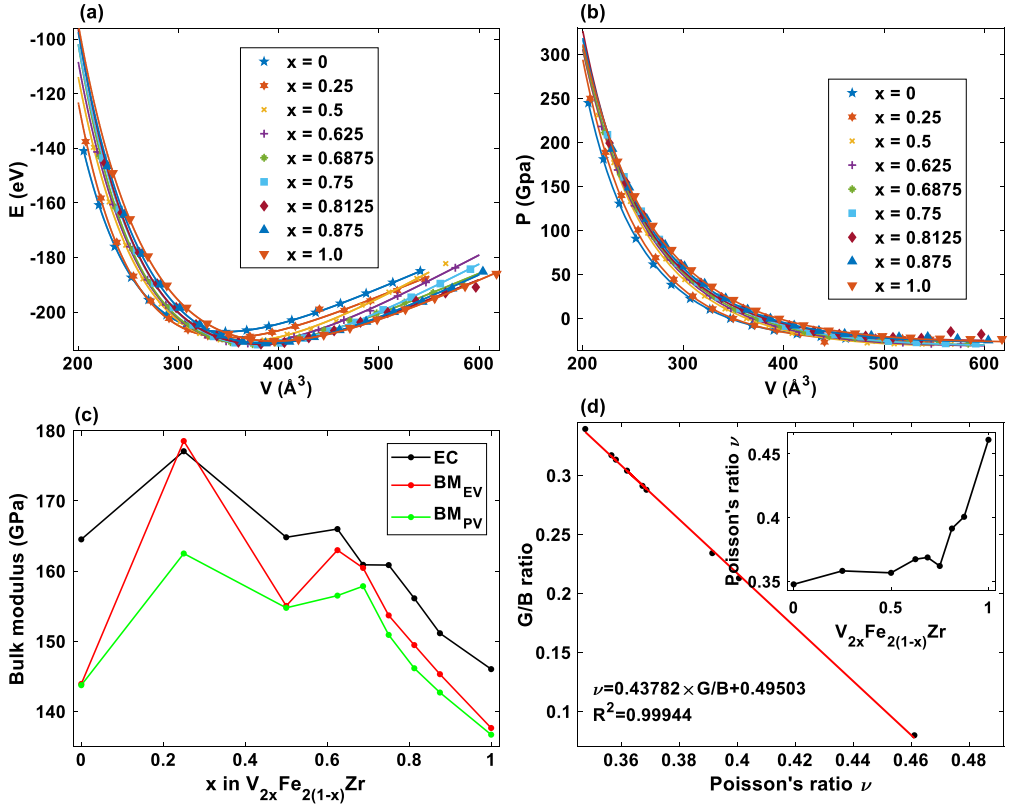

Fig. 6. (a) Total energies and (b) pressures of $V_{2x}Fe_{2(1-x)}Zr$ alloy systems as the function of volumes obtained by fitting each group data into BM equation, respectively. (c) Bulk modulus versus the vanadium contents; (d) Linear relationship of G/B values upon Poisson's ratio in target alloy systems.

indicating the reliability for a prediction of mechanical strength of these alloy systems.

Bulk modulus gives a description of the elasticity of homogeneous isotropic solids that can be expressed as the force per unit area and the incompressibility of the solid. The bulk modulus of $V_{2x}Fe_{2(1-x)}Zr$ calculated from different methods as shown in Fig. 6(a) are close with a variation range between 135 GPa and 178 GPa. Although there is a generally large difference in

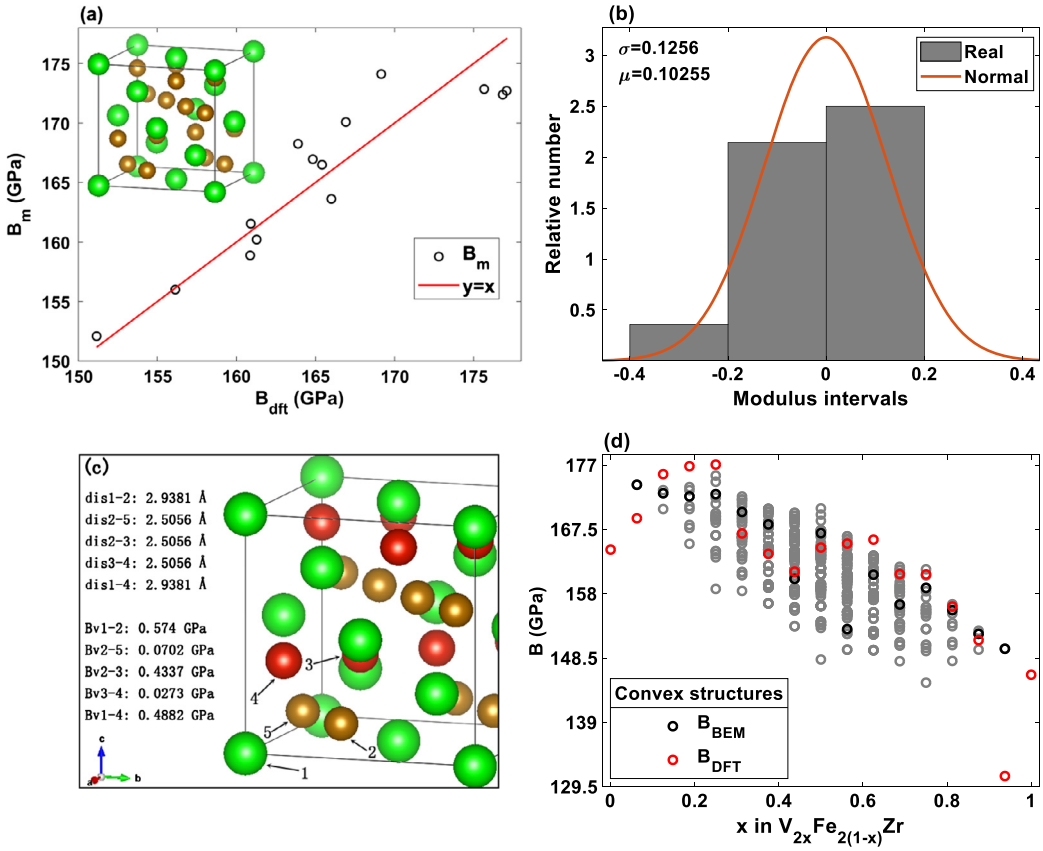

Fig. 7. (a) Bulk modulus of stable $V_{2x}Fe_{2(1-x)}Zr$ alloy structures (cubic lattice illustrated in left-top) calculated from elastic constants (DFT) that are fitted to BEM method; (b) difference characteristics of bulk modulus calculated between elastic constants and BEM; (c) Distance and bulk modulus among the V, Fe and Zr three atoms belonging first neighbor in the supercell of 4 times primitive one; (d) Bulk modulus of 531 unequivalent supercells expanded as 4 times volume of primitive cell.

the calculation results of the elastic modulus, this elastic result is close to those being reported in the literature [35–40]. Notably, the elastic modulus of the structures with intermediate substitution concentrations $V_{2x}Fe_{2(1-x)}Zr$ (obviously at the stoichiometry of $V_{0.5}Fe_{1.75}Zr$) are greater than those of V_2Zr and Fe_2Zr, exploring the production of V-Fe-Zr ternary alloys possessing with a lighter weight and higher elastic modulus to improve industrial quality of engineering application.

The ratio of shear modulus to bulk modulus is found to have a linear relationship with the Poison's ratio as shown in Fig. 6(d) (the inset conveys variable of Poison's ratio along V concentration in target alloy), revealing the plastic strength by increasing Poison's ratio with larger V concentrations induced by the degree of bond and directionality within a designed alloy. S. F. Pugh [41] et al. put forward an empirical criterion to tell the strength of ductility or brittleness in one material by the ratio of shear modulus to bulk modulus with a boundary of 0.57, viz. a ratio greater than 0.57 indicates a brittle property but lower than that matches a ductile feature, the higher the ratio, the stronger the brittleness and vice versa. In this calculation all $V_{2x}Fe_{2(1-x)}Zr$ alloy systems hold G/B value less than 0.57 and thus are ductile naturally.

Similar to the BEM, we have attempted to fit the elastic modulus with various bonds. Fig. 7(a) shows the bulk modulus from the model prediction and those from the first-principles method (B_{DFT}) respectively, in which Fe atoms are replaced by V atoms sequentially from one to fourteen in a four times supercell. Fig. 7(b) shows the normal distribution between the B_M and B_{DFT} with good distribution characteristics of small standard deviation and average. As listed in Fig. 7(c), the largest modulus taken up Fe-Zr metal bond implicates the highest contribution of Fe atom to the bulk modulus in the alloy crystal, while according to the modulus results mentioned above, the structures with largest bulk modulus compose of initial V contents, which may be due to an increase in the whole stiffness of alloy structure that is arisen from the advantage of isotropic strength brought by the substitution of V to Fe atom. The model predicted bulk moduli are found to be insistent with those from DFT, indicating a fast evaluation of elastic properties and a preventing for unnecessary cost of computation resource and time.

The elastic anisotropy is commonly considered as an important factor in scrutinizing the effects of micro-cracks and lattice distortion on the mechanical properties of materials. A surface construction is essential due to the fact that the bulk modulus, as the Young's modulus mentioned above is inefficient to describe the elastic behaviors of a crystal completely. For instance [19,42,43], the modulus in the cubic lattice are calculated as below:

$$\frac{1}{B} = S_{11} + 2S_{12} \tag{4}$$

$$\frac{1}{E} = S_{11} - 2(S_{11} - S_{12} - S_{44}/2)(l_1^2 l_2^2 + l_2^2 l_3^2 + l_1^2 l_3^2) \tag{5}$$

Where $l_i (i = 1, 2, 3)$ is direction cosine in any arbitrary directions, and is expressed respectively as $l_1 = sin\theta \cdot cos\varphi$ $(0 \le \theta \le \pi;$ $0 \le \varphi \le 2\pi)$, $l_2 = sin\ \theta \cdot sin\varphi$, and $l_3 = cos\varphi$ in a spherical coordinate. According to 3D surfaces of Young's modulus shown in Fig. 8, the map should be spherical for an isotropic crystal and any deviation from the spherical shape corresponds to an anisotropic elasticity in the direction. The structures of $V_{0.5}Fe_{1.5}Zr$ and V_2Zr

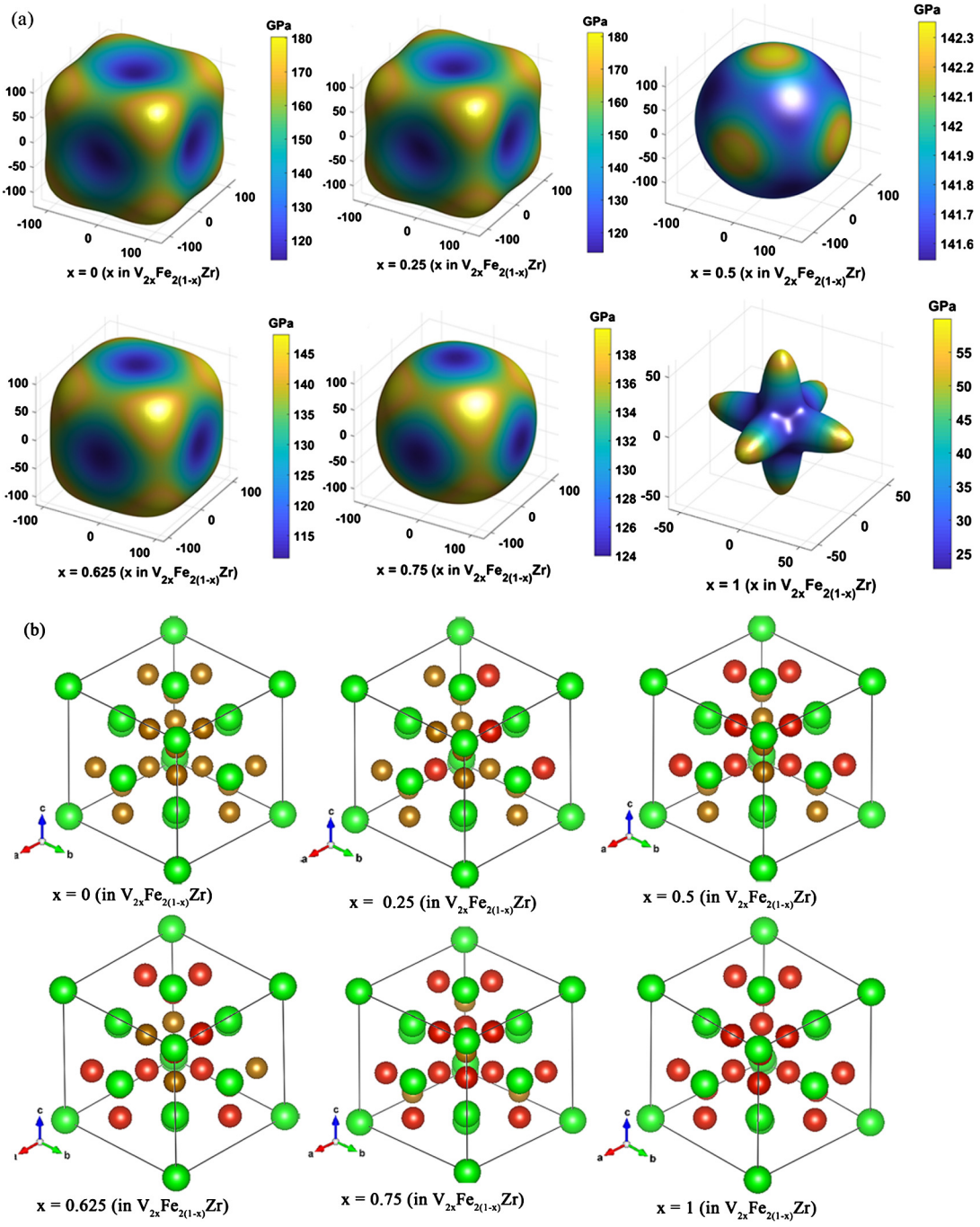

Fig. 8. Topological diagrams (a) of anisotropy degree in $V_{2x}Fe_{2(1-x)}Zr$ selective alloy crystal structures (b) along an increase in the substitution concentration of V.

show an opposite anisotropic trend, while the ZrFeV shows the greatest degree of isotropic elasticity, the replacement of V to Fe can neutralize anisotropic property of alloy structure thus make it tend to become isotropic.

As shown in Fig. 9(a), stable structures on the convex-hull line for no spin polarization were $V_{0.5}Fe_{1.5}Zr$, VFeZr, $V_{1.25}Fe_{0.75}Zr$, $V_{1.375}Fe_{0.625}Zr$, $V_{1.5}Fe_{0.5}Zr$, $V_{1.625}Fe_{0.375}Zr$, $V_{1.75}Fe_{0.25}Zr$, while $V_{0.5}Fe_{1.5}Zr$ is not stable according to the spin polarization. Moreover, the formation entropies of the given structure from spin polarized calculations are lower than those without spin polarization. Thus, the magnetization will affect the stability of the $V_{2x}Fe_{2(1-x)}Zr$ alloy.

Fig. 9(b) shows the average atomic magnetic moment in 9 stable structures, as well as the calculated bulk moduli (B) with and without spin polarization. Obviously, magnetic moment decreases with the increasing V contents in the $V_{2x}Fe_{2(1-x)}Zr$ system. It is found that the magnetism of $V_{2x}Fe_{2(1-x)}Zr$ structures is caused by the ferromagnetic Fe atom, while the V and Zr atom possess an antiferromagnetic property and there is $0\mu_B$ for the V_2Zr structure. On the other hand, the deformation of lattice will induce elastic potential energy, leading to the abnormality of elastic constant within substituted structures. Note that the calculated bulk moduli of Fe_2Zr with and without spin polarization are 164.5 GPa and 204.4 GPa, respectively. The results for V_2Zr are 146.0 GPa and 138.8 GPa, respectively. Thus, the magnetization will also affect the elastic properties of the $V_{2x}Fe_{2(1-x)}Zr$ alloy. In addition, the electronic properties (shown in Fig. 5) are from the spin polarized calculations.

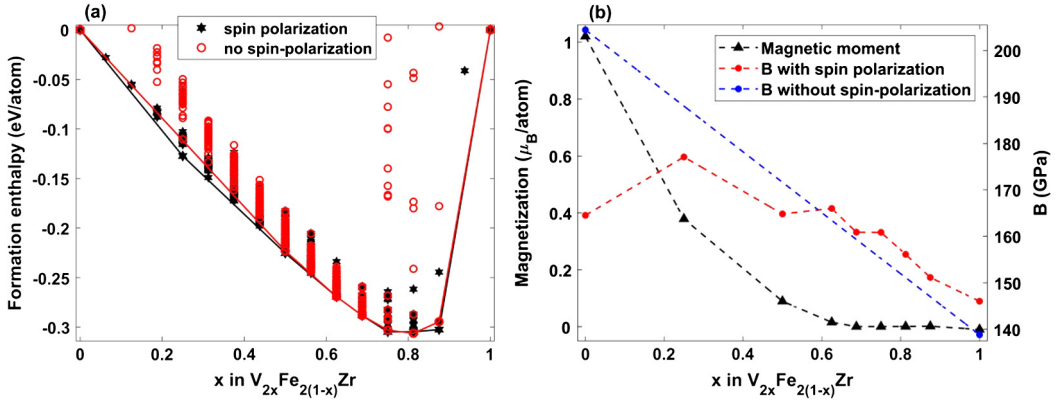

Fig. 9. (a) Formation entropy of the $V_{2x}Fe_{2(1-x)}Zr$ system (all inequivalent cubic structures of 4 times of primitive unit cell) calculated with and without spin polarization respectively; (b) Magnetic moment and bulk moduli (denoted as B, and which was calculated by the elastic constants obtained under spin condition and not under it respectively) of $V_{2x}Fe_{2(1-x)}Zr$ system in stable structures.

4. Conclusion

In summary, we have theoretically investigated the $V_{2x}Fe_{2(1-x)}Zr$ and $Sc_xY_{1-x}Fe_2$ based on the first-principles calculations. The $V_{2x}Fe_{2(1-x)}Zr$ alloy is energetically favorable stable according to the convex analysis at low temperature, while the $Sc_xY_{1-x}Fe_2$ system become miscible at the temperature above 700 °C, which is in good agreement with experimental results. With the bond energy model, we have shown that the binding energy of V and Fe to the Zr atom is dominant to the total energies with the complete miscibility of V/Fe atoms, which is in consistence of the ELF and PDOS analysis. Similarly, the bulk modulus can be also fit with the number of various bonds, and the introduction of V species makes the bulk modulus of the alloy structure higher than that of pure end-point structure, up to the maximum of 178 GPa, improving its mechanical strength and homogenization. This study offers researchers a better understanding for the structural stability and mechanical strength of V-Fe-Zr and Sc-Y-Fe ternary alloys, and provides theoretical guidance for the design and product of high-entropy alloys with related components and compositions.

Declaration of competing interest

The authors declare that they have no known competing financial interests or personal relationships that could have appeared to influence the work reported in this paper.

Acknowledgements

The financial support by the MOST Scientific Project (2018YFB1502101) and the National Natural Science Foundation of China (Grant Nos. U1601212), as well as the XRD data provider from the School of Materials Science and Engineering and Guangdong Provincial Key Laboratory of Advanced Energy Storage Materials, South China University of Technology, Guangzhou, 510641, China, are acknowledged.

References

[1] Y.-G. Yao, Z.-N. Huang, P.-F. Xie, S.D. Lacey, R.J. Jacob, H. Xie, F.-J. Chen, A. Nie, T.-C. Pu, M. Rehwoldt, D.-W. Yu, M.R. Zachariah, C. Wang, R.S. Yassar, J. Li, L.-B. Hu, Carbothermal shock synthesis of high-entropy-alloy nanoparticles, Science 359 (6383) (2018) 1489–1494.

[2] K. Takeuchi, R. Tanaka, K. Yuge, New Wang-Landau approach to obtain phase diagrams for multicomponent alloys, Phys. Rev. B 96 (2017) 144202.

[3] X.-W. Liang, S.-T. Zhao, C.-C. Shao, A. Bergara, H.-Y. Liu, L.-Y. Wang, R.-X. Sun, Y. Zhang, Y.-F. Gao, Z.-S. Zhao, X.-F. Zhou, J.-L. He, D.-L. Yu, G.-Y. Gao, Y.-J. Tian, First-principles study of crystal structures and superconductivity of ternary YSH_6 and $LaSH_6$ at high pressures, Phys. Rev. B 100 (18) (2019) 184502.

[4] S.-K. Wang, C.-D. Ren, H.-Y. Tian, J. Yu, M.-L. Sun, MoS_2/ZnO van der Waals heterostructure as a high-efficiency water splitting photocatalyst: a first-principles study, Phys. Chem. Chem. Phys. 20 (2018) 13394–13399.

[5] Y. Pan, W.-M. Guan, Y.-Q. Li, Insight into the electronic and mechanical properties of novel TMCrSi ternary silicides from first-principles calculations, Phys. Chem. Chem. Phys. 20 (2018) 15863–15870.

[6] N. Karuppanan, S. Kalainathan, A new nonlinear optical stilbazolium family crystal of (E)-1-Ethyl-2-(4-nitrostyryl) Pyridin-1-ium Iodide: synthesis, crystal structure, and its third-order nonlinear optical properties, J. Phys. Chem. C 122 (8) (2018) 4572–4582.

[7] A. Onwubiko, W. Yue, C. Jellett, M.-F. Xiao, H.-Y. Chen, M.K. Ravva, D.A. hanifi, A.C. Knall, B. Purushothaman, M. Nikolka, J.C. Flores, A. Salleo, J.L. Bredas, H. Sirringhaus, P. Hayoz, L.M. Culloch, Fused electron deficient semiconducting polymers for air stable electron transport, Nat. Commun. 416 (2018).

[8] S.B. Gesari, M.E. Pronsato, A. Visintin, A. Juan, Hydrogen storage in AB_2 laves phase (A = Zr, Ti; B = Ni, Mn, Cr, V): binding energy and electronic structure, J. Phys. Chem. C 114 (2010) 16832–16836.

[9] V.P. Boncour, M. Guillot, O. Isnard, B. Ouladdiaf, A. Hoser, T. Hansen, N. Stusser, Interplay between crystal and magnetic structures in $YFe_2(H_\alpha D_{1-\alpha})_{4.2}$ compounds studied by neutron diffraction, J. Solid State Chem. 245 (2017) 89–109.

[10] S.-R. Yuan, L.-Z. Ouyang, M. Zhu, Y.-J. Zhao, Theoretical study of YFe_2H_x (x = 0–5): a comparison between cubic and orthorhombic phases, J. Magn. Magn. Mater. 460 (2018) 61–68.

[11] C.A. Biffi, A.G. Demir, M. Coduri, B. Previtali, A. Tuissi, Laves phases in selective laser melted $TiCr_{1.78}$ alloys for hydrogen storage, Mater. Lett. 226 (2018) 71–74.

[12] Z.-D. Yao, X.-Z. Xiao, Z.-Q. Liang, X. Huang, H.-Q. Kou, W.-H. Luo, C.-G. Chen, L.-J. Jiang, L.-X. Chen, Study on the modification of Zr-Mn-V based alloys for hydrogen isotopes storage and delivery, J. Alloys Compd. 797 (2019) 185–193.

[13] H.-L. Pang, Z.-M. Li, C. Zhou, H. Wang, L.-Z. Ouyang, S.-R. Yuan, Y.-J. Zhao, M. Zhu, Achieving the dehydriding reversibility and elevating the equilibrium pressure of YFe_2 alloy by partial Y substitution with Zr, Int. J. Hydrog. Energy 43 (31) (2018) 14541–14549.

[14] S. Banerjee, A. Kumar, C.G.S. Pillai, Improvement on the hydrogen storage properties of $ZrFe_2$ Laves phase alloy by vanadium substitution, Intermetallics 51 (2014) 30–36.

[15] Z.-J. Cao, L.-Z. Ouyang, H. Wang, J.-W. Liu, L.-X. Sun, M. Felderhoff, M. Zhu, Development of Zr-Fe-V alloys for hybrid hydrogen storage system, Int. J. Hydrog. Energy 41 (26) (2016) 11242–11253.

[16] M. Budzyński, J. Sarzyński, M. Wiertel, Z. Surowiec, Effect of Sc substitution for Y on structural properties and hyperfine interactions in $Y_{1-x}Sc_xFe_2$ compounds, Nukleonika 48 (Supplement 1) (2003) S79–S83.

[17] J. Štrof, J. Pavlů, U.D. Wdowik, J. Buršík, M. Šob, J. Vřešťál, Laves phases in the V–Zr system below room temperature: stability analysis using ab initio results and phase diagram, Calphad 44 (2014) 62–69.

[18] D. Chattaraj, C. Majumder, S. Dash, Structural, electronic, elastic and thermodynamic properties of Zr_2Fe and Zr_2FeH_5: a comprehensive study using first principles approach, J. Alloys Compd. 615 (2014) 234–242.

[19] K. Ali, A. Arya, P.S. Ghosh, G.K. Dey, A first principles study of cohesive, elastic and electronic properties of binary Fe–Zr intermetallics, Comput. Mater. Sci. 112 (2016) 52–66.

[20] G. Kresse, J. Furthmüller, Efficient iterative schemes for ab initio total-energy calculations using a plane-wave basis set, Phys. Rev. B 54 (16) (1996).

[21] G. Kresse, D. Joubert, From ultrasoft pseudopotentials to the projector augmented-wave method, Phys. Rev. B 59 (3) (1999).

[22] G. Trimarchi, A.J. Freeman, A. Zunger, Predicting stable stoichiometries of compounds via evolutionary global space-group optimization, Phys. Rev. B 80 (2009) 092101.

[23] X.-B. Yang, J. Ni, Ground states of potassium adsorbate on single-walled carbon nanotubes, Phys. Rev. B 67 (2003) 195403.
[24] Z.-G. Xia, G.-K. Liu, J.-G. Wen, Z.-G. Mei, M. Balasubramanian, M.S. Molokeev, L.-C. Peng, L. Gu, D.J. Miller, Q.-L. Liu, K.R. Poeppelmeier, Tuning of photoluminescence by cation nanosegregation in the $(CaMg)_x(NaSc)_{1-x}Si_2O_6$ solid solution, J. Am. Chem. Soc. 138 (4) (2016) 1158–1161.
[25] J.-A. Chan, J.-Z. Liu, A. Zunger, Bridging the gap between atomic microstructure and electronic properties of alloys: the case of (In, Ga)N, Phys. Rev. B 82 (4) (2010) 045112.
[26] A.D. Becke, K.E. Edgecombe, A simple measure of electron localization in atomic and molecular systems, J. Chem. Phys. 92 (1990) 5397.
[27] B. Silvi, A. Savin, Classification of chemical bonds based on topological analysis of electron localization functions, Nature 371 (1994) 683–686.
[28] G. Yuan, S.-X. Huang, J.-J. Niu, S. Qin, X. Wu, H.-R. Ding, A.-H. Lu, Compressibility of Cs_2SnBr_6 by X-ray diffraction and Raman spectroscopy, Solid State Commun. 275 (2018) 68–72.
[29] S.-L. Shang, Y. Wang, D.E. Kim, Z.-K. Liu, First-principles thermodynamics from phonon and Debye model: application to Ni and Ni_3Al, Comput. Mater. Sci. 47 (2010) 1040–1048.
[30] S.-L. Shang, Y. Wang, Z.-K. Liu, First-principles elastic constants of α- and θ-Al_2O_3, Appl. Phys. Lett. 90 (2007) 101909.
[31] C.M. Kube, M.d. Jong, Elastic constants of polycrystals with generally anisotropic crystals, J. Appl. Phys. 120 (16) (2016) 165105.
[32] Y. Wang, J.-J. Wang, H. Zhang, V.R. Manga, S.-L. Shang, L.-Q. Chen, Z.-K. Liu, A first-principles approach to finite temperature elastic constants, J. Phys. Condens. Matter 22 (22) (2010) 225404.
[33] P. Ravindran, L. Fast, P.A. Korzhavyi, B. Johansson, Density functional theory for calculation of elastic properties of orthorhombic crystals: application to $TiSi_2$, J. Appl. Phys. 84 (9) (1998) 4891–4904.
[34] S.U. Rehman, F.K. Butt, B. Ul Haq, S. AlFaify, W.S. Khan, C.-B. Li, Exploring novel phase of tin sulfide for photon/energy harvesting materials, Sol. Energy 169 (2018) 648–657.
[35] X.-Y. Zhang, L. Chen, M.-Z. Ma, Y. Zhu, S.-H. Zhang, R.-P. Liu, Structural, elastic, and thermal properties of Laves phase ZrV_2 under pressure, J. Appl. Phys. 109 (2011) 113523.
[36] C.-W. Zhang, Electronic structure and bonding properties for Laves-phase RV_2 (R=Ti, Nb, Hf, and Ta) compounds, Physica B, Condens. Matter 403 (12) (2008) 2088–2092.
[37] F.-M. Chu, M. Šob, R. Siegl, T.E. Mitchell, D.P. Pope, S.P. Chen, Total energy and electronic structure calculations of C15 Laves-phase compounds MV_2 (M=Zr, Hf or Ta): elastic properties, Philos. Mag. B 70 (4) (1994) 881–892.
[38] K. Benayed, A. Settouf, N. Benkhettou, D. Rached, B. Abidri, Electronic and magnetic properties of AFe_2 (A=Zr, Hf, Lu) compounds in the cubic Laves phase, Physica B, Condens. Matter 551 (2018) 152–162.
[39] K. Ali, P.S. Ghosh, A. Arya, A DFT study of structural, elastic and lattice dynamical properties of Fe_2Zr and $FeZr_2$ intermetallics, J. Alloys Compd. 723 (2017) 611–619.
[40] R. Kuentzler, Y. Dossmann, Electronic, lattice and superconducting properties of the Zr-Fe compounds-comparison with their amorphous counterparts, Phys. Lett. A 118 (4) (1986) 213–217.
[41] S.F. Pugh XCII, Relations between the elastic moduli and the plastic properties of polycrystalline pure metals, Philos. Mag. 45 (367) (1954) 823–843.
[42] P.P. Ferreira, T.T. Dorini, F.B. Santos, A.J.S. Machado, L.T.F. Eleno, Elastic anisotropy and thermal properties of extended linear chain compounds MV_2Ga_4 (M = Sc, Zr, Hf) from ab-initio calculations, Materialia 4 (2018) 529–539.
[43] R. Golesorkhtabar, P. Pavone, J. Spitaler, P. Puschnig, C. Draxl, ElaStic: a tool for calculating second-order elastic constants from first principles, Comput. Phys. Commun. 184 (2013) 1861–1873.